

# Main Belt Asteroids

Banan Yamani

Submitted: January 10, 2024

Nestled between the orbits of Mars and Jupiter lies the main asteroid belt, an area rich in relics from the early solar system. The orbital parameters of a number of major belt asteroids are thoroughly examined in this project, with an emphasis on the asteroids Helio, Marion, Kallisto, Deborah, Themis, Eurykleia, and Aneas. The FindOrb software and sophisticated observational methods were utilized to model the entire orbits of these asteroids. Among the main findings are the highest semi-major axis of the Jupiter Trojan Aneas, 5.23 AU, indicates that it orbits are further from the Sun. Through the acquisition of multiple photographs of the asteroid Marion from Durham and La Palma, the astronomical unit was calculated to be only 37.5 % higher than the standard value. It was measured as  $1.375 \pm 0.227$  AU or 205 712 032 000km. The trajectories of these celestial bodies were then modeled using the Monte Carlo method, which produced 300 distinct positions by altering the orbital parameters. This is because the goal of this research is to improve knowledge of their orbital dynamics so that a mission to one of these asteroids can be completed. Evaluating these parameters is critical to future position prediction, improved navigational accuracy for future space missions, and historical insights into the processes that shaped the main belt's current configuration.

## I. INTRODUCTION

### A. History

Nestled between the orbits of Mars and Jupiter lies a region teeming with the remnants of the early cosmos—the Main Belt. Stretching approximately between 2.1 and 3.3 astronomical units from the Sun, this celestial zone is home to a multitude of asteroids. These small, rocky bodies, varying in size from tiny dust particles to the colossal Ceres, weave through space in their unique elliptical orbits (Marcos, Marcos 2022) and are composed of left-over material from the birth of the solar system. The Main Belt is the vastest area between Mercury and Neptune that does not contain a planet, and it also acts as a boundary between the gaseous and rocky planets (Raymond, Nesvorný 2020). When discussing the origins of main belt asteroids, there are two opposing points of view. The planetesimals that made up the belt could have had masses several times greater than Earth's, and their mass could have been reduced by a factor of 1000 to reach the current estimated mass. Alternatively, planetesimals from different regions of the Sun's planet-forming disk eventually filled the belt, which had formed with little to no mass at all. Three general possibilities can be identified for the evolution of the asteroid belt. It's possible that a planet the size of Jupiter moved through the asteroid belt, dispersing material. There is another conjecture that this planet traveled inward, but it did not actually pass through the main belt of asteroids but instead remained close to it. According to the most recent conjectures, this massive planet split apart to form a dense belt instead of migrating at all. A vast spectrum of orbital eccentricities and inclinations is produced by the dynamical excitation of asteroid orbits. Moreover, the compositions of asteroids vary, with a tendency for the inner belt to include more arid objects and the outer belt to contain more water-rich objects (Liu, Wu 2023). We define the outer edge of the asteroid belt at the location of the 2:1 mean motion resonance with the giant planet Jupiter. In the solar system, this is at about 3.3 AU from the Sun. In this region, the asteroid belt formed due to perturbations and collisions from the outer giant planet, which led to disintegration rather than accretion. The inner edge of the asteroid belt is not as well defined. It must be at the radius where planet formation can continue since the disturbances from the massive planet get smaller. We consider the inner edge to be around the orbit of Mars

at roughly 1.5 AU (Martin, Livio 2020). Jupiter's gravity has played a significant impact in the Main Belt's history. The accretion process in the belt was disturbed by the giant planet's gravitational pull, preventing the development of a planet. The smaller asteroids that we see today are the result of the collision and breakup of several proto-planetary bodies caused by this influence. The history of the Main Belt is dynamic and characterized by multiple collisions. These encounters have fractured and split asteroids over billions of years, resulting in smaller bodies and families of asteroids with comparable orbits and properties.

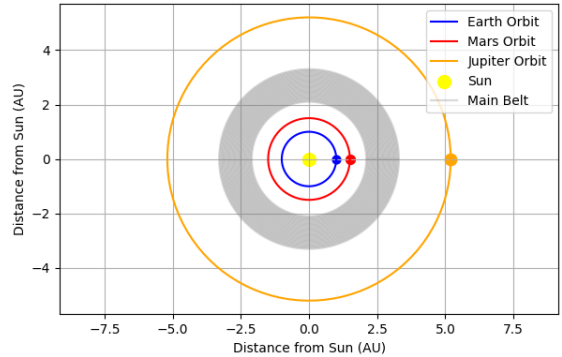


**FIG. 1:** A simplified illustration of the Inner Solar System. This graphic shows the region of the Main Belt asteroids relative to the positions and orbits of Earth, Mars, and Jupiter. Data extracted from NASA'S Jet Propulsion Laboratory.

### B. Structure & Classification

The visual magnitude of an asteroid can be obtained using ground-based observations. Using the visual magnitude, a value of the absolute magnitude (the visual magnitude that it would have if it were at 1 AU from both the Sun and the observer) can be derived as well as the size and shape of the object. An asteroid's spectral characteristics also reveal details about its composition. Using spectroscopy ranging from visible light to near-infrared, asteroids have been classified into various taxonomic groups according to the features of their spectroscopic signature at various wavelengths. Taxonomic type S asteroids are pri-

marily found in the inner main belt, with an average visual albedo (the reflectivity of a surface) of  $p_v$  0.15. They have distinct silicate absorption bands and are several times brighter than C-type asteroids (visual albedo  $p_v$  0.05 on average), which are mostly found in the outer main belt. The materials that make up ordinary chondrites, the most common type of meteorite, which are moderately evolved but unmelted chondritic rocks, are likely similar to those of S-type asteroids. Numerous subgroups make up the entire taxonomy of asteroids, including the B, C, P, and D types, which are all associated with dark, reddish asteroids. These asteroids most likely consist of silicate minerals, reduced iron, and other metals, as well as complex organic molecules, similar to the carbonaceous chondrites, the most primitive type of meteorites. D-type asteroids have no obvious relationship to any type of meteorite and are notably red at long infrared wavelengths. They may also be rich in organic compounds. Originally, it was believed that metallic fragments from differentiated planetary cores belonged to a distinct class called M. The mineralogy of some M-type asteroids, however, most likely corresponds to hydrated silicate rather than metal, according to mid-infrared spectroscopy. Thus, our comprehension of composition based exclusively on spectral observations remains uncertain and may not enable us to identify a potential overall heterogeneity. (Michel 2014) We can narrow down the characteristics of the asteroid belt's observed structure to four constraints: the belt's very low total mass, orbital structure of the belt, anatomical structure of the belt, and asteroid size frequency distribution. The majority of the belt's mass is distributed as follows:

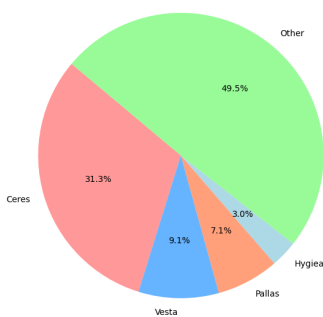


**FIG. 2:** Mass Distribution of the Main Belt

Throughout the main belt, asteroid orbits exhibit modest variations, with eccentricities of  $0 < e < 0.3$  and inclinations of  $0 < i < 20$ . Beyond the Kirkwood gaps, resonances, and clumps connected to asteroid families, the belt contains other substructures. Taxonomy indicates that S-types (silicate) predominate in the inner main belt and C-types (carbonaceous) in the outer main belt. Outside the outer main belt, D-types (dark) are more common. Much of the mass of the belt is contained in the top-heavy asteroid size-frequency distribution (SFD), which means a higher frequency of larger asteroids compared to smaller ones. (Raymond, Nesvorný 2020) Many meteorites found on Earth are believed to have originated from the Main Belt, knocked out of their orbit by collisions or gravitational interactions and eventually finding their way to Earth. Studying these meteorites has provided direct insights into the

composition and history of the Main Belt asteroids.

Another way of categorizing main belt asteroids is by family. Usually, asteroid families are distinguished by their shared orbital characteristics, such as semi-major axis, eccentricity, and inclination. These similarities point to a shared origin, which is typically a larger parent body that broke apart as a result of a collision. When the pieces of the family that were formed during the impact event scatter so widely due to gravitational or non-gravitational forces, the family is no longer recognizable as a unit, and they "die.". Examples of families that exist in the outer main belt are the Themis, Meliboea, and Ursula families. (Carruba 2016).

Asteroids present in the solar system can also be classified based on their location. While this research focuses on Main Belt asteroids, there are also Trojan asteroids and Near Earth asteroids (NEAs). Although Trojan asteroids circle a larger planet, they avoid collisions with it because of two unique locations in the orbit known as the L4 and L5 Lagrangian points. There, a Trojan's propensity to fly out of orbit otherwise balances the gravitational pull of the planet and the Sun. The largest group of Trojan asteroids consists of Jupiter Trojans. They are estimated to be as numerous as the asteroid belt's asteroids. Near-Earth asteroids are celestial bodies found in close proximity to Earth on their orbits. "Earth-crossers" are asteroids that actually go through Earth's orbit (NASA). Astronomers constantly monitor them in order to be aware of those that penetrate Earth's atmosphere. All the asteroids that may crash into Earth in the future are listed on NASA's "Sentry Impact Risk" list.

### C. Importance

Researching Main Belt asteroids presents a multitude of opportunities and insights, contributing to our understanding of the formation of the solar system, expanding our capacity for orbital modeling, and providing new avenues for resource mining. Due to their composition, which is abundant in metals and other valuable materials, these asteroids could be the focus of space mining projects. We can learn about the distribution of materials in the early solar system and the processes leading to planet formation by examining the elemental composition of these asteroids. A tempting possibility for future resource extraction from some of these asteroids is the presence of metals like iron, nickel, and rare elements like platinum. This could help with space exploration and possibly alleviate Earth's resource scarcity problems.

Moreover, the organic compounds present on a large number of MBAs provide information about the organic chemistry of the early solar system and may shed light on the origins of life. It is equally important to comprehend the orbits of Main Belt asteroids. Precise orbital modeling is essential for multiple purposes. First and foremost, it helps with a crucial component of planetary defense plans: evaluating any possible collision risks these objects might pose to Earth. Secondly, planning space missions—for exploration, science, or mining asteroids—needs accurate knowledge of their trajectories. Thirdly, knowledge of the orbital dynamics of MBAs is vital for understanding solar system gravitational interactions, particularly how large planets affect smaller bodies. Therefore, research on Main Belt asteroids is a multidisciplinary field that contributes to our

understanding of science, has potential economic benefits through space mining, and is essential to the sustainability and safety of space exploration in the future. It's a field that aids in the investigation of the past and prepares us for the exploration and use of space in the future.

#### D. Orbital Parameters

A thorough understanding of orbital parameters and how they define an object's orbit requires familiarity with a few crucial formulas and ideas. By using these formulas, one can translate orbital elements into a physical depiction of an object's orbit around a primary body, such as the Sun or Earth. It is easier to use these elements to characterize and visualize an orbit than it is to do so using position and velocity vectors at a specific epoch (a moment in time used as a reference point for some time-varying astronomical quantity). These are the semi-major axis  $a$ , eccentricity  $e$ , inclination  $i$ , longitude of ascending node  $\Omega$ , argument of periaxis  $\omega$ , and mean anomaly  $M$ . The seventh orbital parameter describes when these parameters are observed or valid, and it is called the epoch time,  $t_o$ .

Semi-major axis represents half of the longest diameter of the elliptical orbit and is the longest radius of an ellipse. This orbital length measurement is commonly used to calculate a body's orbital period in celestial mechanics. It is also defined as the distance between the sun and the object. Eccentricity provides us with the orbit's shape. A perfect circle has an eccentricity of 0, and ellipses that are progressively longer have an eccentricity between 0 and 1. A parabolic trajectory would be represented by an eccentricity exactly equal to 1, and a hyperbolic trajectory by a value greater than 1. Inclination indicates how tilted the orbit's plane is with respect to a reference plane. The plane of the Solar System, commonly referred to as the reference plane for objects orbiting the Sun, is known as the ecliptic plane. Longitude of ascending node specifies the orbits orientation in the reference plane. When an orbiting body crosses the reference plane from south to north, it is said to be ascending node. Measured in the reference plane, it is the angle formed by the ascending node's direction and a reference direction known as the vernal point. Argument of periaxis, measured both in the orbital plane and in the direction of motion, is the angle from the ascending node to the orbit's point of closest approach to the primary body (periaxis). It is common to refer to this point as the perihelion for orbits around the Sun. Lastly, mean anomaly represents a time measure. It indicates the orbiting body's position along its path at a particular moment in time. The mean anomaly begins at the periaxis and increases uniformly from 0 to 360 degrees during each orbit.

An orbit's size and form are determined by its semi-major axis and eccentricity. Thus, in the orbital plane, the spacecraft's motion is defined by these two orbital elements. In three dimensions, the orbit's orientation is defined by the second set of orbital elements. The tilt of the orbit plane relative to the equatorial plane, or inclination, ranges from  $0^\circ$  to  $180^\circ$ . An orbit is considered direct or pro-grade (easterly direction) for values of  $0 \leq i < 90$ , retrograde (westerly orbit) for values of  $90 < i \leq 180$ , and polar for values of  $i = 90$ . In the equatorial plane, the longitude of the ascending node is measured counterclockwise. The periaxis (or perigee, in the case of earth orbits) argument is quantified

in the direction of the asteroid's motion.

The Mean Anomaly is the only one of the six classical orbital elements that changes over time by nature. With each orbit, this element completes a full cycle by showing the position of the orbiting body within its orbit at a given time and changing linearly with time. For a given orbit, the other components usually don't change unless outside forces cause them to. For example, especially in multi-body systems, slow changes in the argument of periaxis and the longitude of the ascending Node can be caused by gravitational interactions with other celestial bodies. On the other hand, when compared to the Mean Anomaly's regular progression, these changes are typically smaller and less predictable. (Catling, Leovy 2007)

#### E. Project Overview

Over the course of three months, this study planned to carry out in-depth observational studies of seven main belt asteroids of choice: Helio, Aneas, Kallisto, Marion, Deborah, Eurykleia and Themis. This research can be divided into 4 main phases: the extraction of coordinates by undergoing a series of ground-based observations, calculating the orbital parameters, creating a predictive model, and analyzing our data by comparing it to JPL Horizon values. The final phase includes using the distance to one of our asteroids to determine a value of the AU.

This observational campaign's main goal was to precisely document these celestial bodies' coordinates in order to gather positional data as they moved across the night sky so that a visualisation of their orbits can be plotted. The coordinates used are the right ascension, a longitude-like coordinate usually written as  $RA$ , and the declination, a latitude-like coordinate usually referred to as  $Dec$ . Declination is expressed in degrees, + and - refer to north and south, respectively. The celestial equator is  $0^\circ$  DEC, and the poles are  $+90^\circ$  and  $-90^\circ$ . RA can be expressed in degrees, but it is more common to specify it in hours, minutes, and seconds of time: the sky appears to turn  $360^\circ$  in 24 hours, or  $15^\circ$  in one hour. So an hour of RA equals  $15^\circ$  of sky rotation (NASA Reference Systems). High-resolution telescopic arrays and astronomical methods had to be used for this project in order to guarantee the precision and dependability of the data gathered. The project's emphasis switched to a thorough analysis phase after the positional data-sets had been compiled. Here, the collected data was processed to determine each asteroid's orbital parameters, including its semi-major axis, eccentricity, inclination, ascending node's longitude, periaxis argument, and mean anomaly. It is essential to extract these orbital parameters because they capture the essential features that define the orbit of each asteroid. The creation of comprehensive orbital models for every asteroid that has been observed will be the project's final product. These models will contribute to a wider understanding of the collective behavior and interactions of these asteroids within the main asteroid belt, in addition to facilitating a deeper understanding of the individual orbital dynamics and behaviors of these asteroids. In order to precisely predict future positions and trajectories, the modeling phase will make use of advanced computational techniques and the laws of celestial mechanics.

Asteroid	Period (Years)	Diameter(km)	Spectral	Type
Helio	5.75	109.60	B	Outer Belt
Aneas	11.96	118.0	D	Jovian Trojan
Kallisto	4.38	48.60	S	Middle Belt
Deborah	4.74	60.10	B	Middle Belt
Marion	5.31	105.90	X	Outer Belt
Eurykleia	4.90	93.10	Ch	Outer Belt
Themis	5.59	198.0	C	Outer Belt

**TABLE I:** Astronomical characteristics of the selected asteroids.

Data extracted from Lowell Minor Planet Services

### F. Parallax

Astronomers have used the idea of parallax to calculate distances to planets such as the Moon, the Sun, and other celestial bodies. Parallax is the object's apparent shift in position when viewed from various angles. Astronomers usually notice this by observing how an object in space seems to move as it revolves around a background of more distant stars as Earth orbits the Sun (Thabeb 2013). Historically, calculating the distance to the Moon was one of the first applications of parallax in astronomy. Astronomers could determine the Moon's distance by using basic trigonometry to measure the angle of the Moon's position with respect to far-off stars from two separate locations on Earth. Using this method, a right triangle is formed, with the angles being the parallax angles determined from the two Earthly observation points and the baseline being the distance between them. The Astronomical Unit (AU), or the average distance between Earth and the Sun, was established with the aid of the concept of parallax, which was also crucial in determining the distance to the Sun.

Eratosthenes may have arrived at a very accurate value of 149 million km as early as ancient Greece, according to some evidence. The first indisputable successful measurement, however, would have to wait until 1672, when Giovanni Domenico Cassini and Jean Richer measured Mars' parallax at two separate points on Earth and calculated the AU from that measurement to be 140 million kilometers. For the next 100 years, that value would persist. Measuring one astronomical unit (AU) was made popular by Edmund Halley in the 18th and 19th centuries. The method was based on timing the infrequent transits of Venus, which happen fewer than twice a century. A value of approximately 153 million kilometers was obtained from the transits in 1761 and 1769. (Vanderbei, Belikov 2007)

The most well-known application of parallax to AU measurement occurred during Venus's transit across the solar surface. The exact moment that Venus crossed the Sun was timed by observers at various points on Earth. The AU was determined using the timing variations brought on by the parallax effect. The simplest formula describing parallax is:

$$p = 1/d \quad (1)$$

where  $p$  is the parallax angle in arcseconds and  $d$  is the distance in parsecs. The smaller the parallax angle, the greater the distance to the object. This relation is often used to determine the distance to stars (Siebert 2005). Astronomers utilize parallax in a variety of ways. To begin with, annual parallax which is the apparent shift of a star's

position caused by the Earth's orbit around the sun. It is determined as the angle that the radius of Earth's orbit around the star subtends. Second, the most popular application of parallax in modern astronomy is stellar parallax. Astronomers can determine a star's distance by tracking the apparent change in position over a period of six months, as Earth moves from one side of its orbit to the other. In this research, the triangulation method was used from two different observation points- Durham, England and La Palma, Spain- to form a parallax angle and determine the distance to the asteroid Marion.

Using a simple triangulation method:

$$d = b/2\tan(\theta), \quad (2)$$

where  $d$  is the distance to the object,  $b$  is the baseline (distance between the two observation points), and  $\theta$  is the parallax angle. (Omodaka 2009)

The 20th century offers another instance of the application of parallax measurements that is similar to the approach used in this project. The asteroid Eros was instrumental in Robert d'Escourt Atkinson's precise determination of the astronomical unit, or the mean distance between Earth and the Sun. In 1930–1931, when Eros was at opposition and making a close approach to Earth, Atkinson organized a number of observations from observatories across the world. By taking pictures of Eros against the far-off starry sky, these observatories made it possible to measure the asteroid's parallax precisely. Finding Eros' apparent angular displacement as a result of the different vantage points that Earth's orbit around the Sun provides was the goal of the parallax measurement. This method formed a large geometric triangle with Eros as the vertex and the diameter of Earth's orbit as the baseline. Taking into account Earth's known orbital diameter, the resulting parallax angle enabled Atkinson to use trigonometry to determine the distance to Eros. Moreover, Atkinson calculated the size of the solar system by taking into account the asteroid's clearly defined orbital components and using Kepler's laws, which establish relationships between orbital periods and orbital sizes. This accurate determination of the distance to Eros at opposition consequently yielded a refined value for the astronomical unit, improving the precision of astronomical distance scales and expanding our knowledge of the solar system's dimensions. (Atkinson 1982)

## II. METHOD

Optical observations provide the majority of the information needed to determine the asteroid's position on the celestial sphere at any given time. Specifically, each observation yields two angular measurements, which are typically right ascension (RA) and declination (DEC) in the equatorial reference frame J2000. These measurements are made in relation to nearby reference stars, the positions of which are given by a catalog of reference stars. Generally speaking, the more accurate the observation, the more accurate the star catalog. Using ground-based observations, seven asteroids were observed over the course of three months. 10 observations for all asteroids except Kallisto and Aneas; 9 observations. The exposure time varied for some asteroids depending on their distance from Earth and their luminosity. For six of the asteroids, an exposure time of 8 seconds was utilized, while for Aneas, an exposure time of 30

seconds was required. This is because Aneas is classified as a Jupiter Trojan, and therefore its orbit is distant from Earth as can be seen in Table 1. Selecting the exposure duration involves making a trade-off between catching movement and accumulating light. Short exposures are essential to prevent motion blur and precisely track the positions of fast-moving objects, such as asteroids. When using a CCD (charge-coupled device) camera to take pictures of celestial bodies, the attributes of the object being imaged and the intended result are the main determining factors in selecting between short and long exposure times. When viewed against a starry backdrop, asteroids move rather quickly. An extended exposure would make the asteroid less of a distinct point and more of a streak or blur in the picture. The stars in the sky seem to move as the Earth rotates. In order to maintain the asteroid as the primary focus and avoid star trails in the picture, brief exposure times are necessary. (Raab 2003)

Four exposures were taken each night for each asteroid so that a mosaic of these images could be made. Mosaics are when the four exposures are layered one on top of the other and are used to cancel out any irregularities present in the images caused by dust particles and such on the telescope lens. From the images captured, the RA and Dec were extracted by comparing the relative positions of the asteroids to reference stars in the same field of view. The accuracy of the extracted coordinates depends on the number of stars in the field of view, so observations had to be executed on clear nights. When observing asteroids, the clear "C" filter was utilized due to the kind of observations performed. All colors (red, green, blue, and violet) and the visible spectrum of light can pass through clear filters. This is useful to record an accurate and natural depiction of the color and spectral features of the asteroid. It is possible for different asteroids to have different spectral signatures; by using a clear filter, it can be ensured that no important data is overlooked.

For this project, telescopes with high f-ratios and low pixel scales were required. These are two crucial characteristics that provide information about a telescope's imaging and optical performance. A telescope with a higher f-ratio, f/10, has a smaller field of view and is suitable for observing brighter, smaller, and more detailed objects such as asteroids. The term "pixel scale" refers to the number of arcseconds that one pixel of a CCD in the imaging camera of a telescope covers in the sky. The focal length of the telescope and the actual size of the camera's pixels define the pixel scale. More arcseconds per pixel, or a smaller pixel scale, results in higher-resolution images with finer details discernible. Each pixel is imaging a smaller portion of the sky. (Battistelli 2021) Three telescopes were used in this research, all with f-ratios of 10 and pixel scales between 0.90 and 1.10. These are the characteristics required to observe minor planets and asteroids.

The six classical orbital parameters were computed by using the data entered into the FindOrb software, which included the RA and Dec, epoch time -in decimal date-, observatory code - 995 for Durham, England and 950 for La Palma, Spain and the absolute magnitude. Absolute magnitude represents a celestial object's inherent brightness. Its definition is the apparent magnitude that the object would have if it were situated 10 parsec away from the observer. No matter where the observer is located, the object's absolute magnitude remains constant regardless of its true distance from Earth. Values of the absolute magnitude were evaluated from Nasa's JPL Horizon.

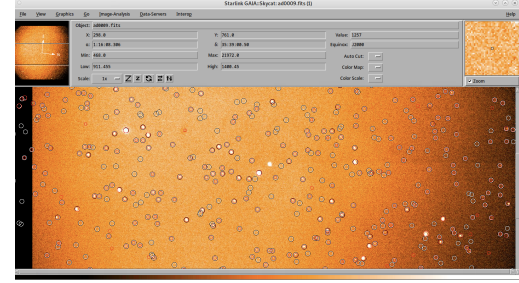


**FIG. 3:** Image of Marion with reference stars according to the "Gaia Sources" and "2Mass" catalogs

#### A. FindOrb

An orbit determination program called "FindOrb" is mainly used to determine comet and asteroid orbits from observational data, including these celestial objects' positions over time. FindOrb uses the input data to estimate the object's orbit in the beginning. This estimate is based on techniques such as the Gauss method, which can generate an initial orbit from as few as three short-duration observations. The orbital elements, which specify the orbit's dimensions, form, and orientation, are produced by FindOrb following its computations. These components can be used to evaluate other aspects, such as the object's potential for close approaches to Earth, create ephemerides (tables of predicted positions), and predict the object's future position. FindOrb uses Gauss' method for orbital determination by making use of a predetermined set of angular observations ( $\alpha_i, \delta_i$ ), such as the object's right ascension and declination on the celestial sphere. These observations are converted into position vectors, and the six classical orbital parameters are found using Gauss's method. In order to perform this transformation, the celestial coordinates must be converted into three-dimensional space vectors, taking into consideration Earth's orbital position at the time of the observations. After establishing these position vectors, the body's velocity vector at one of the observation points is found using a sophisticated combination of geometric and gravitational principles taken from celestial mechanics, specifically Kepler's laws. (Gronchi 2004)

Gauss's f and g series, a polynomial equation that links the position and velocity of the celestial body, is essential to this process. Keep in mind that the expressions are evaluated for  $i = 1$  and  $i = 3$  and are derived up to the fourth order. This is due to the fact that Gauss' method requires a minimum of three observations in order to determine the orbital elements.

$$f_i = 1 - \frac{\tau_i^2}{24r^3} + \left( \frac{\vec{r} \cdot \dot{\vec{r}}}{r^2} \right) \frac{\tau_i^3}{2r^5} + \frac{\tau_i^4}{24r^3} \left[ 3 \left( \frac{\vec{r} \cdot \dot{\vec{r}}}{r^2} - \frac{1}{r^3} \right) - 15 \left( \frac{\vec{r} \cdot \dot{\vec{r}}}{r^2} \right)^2 + \frac{1}{r^3} \right] \quad (3)$$

$$g_i = \tau_i - \frac{\tau_i^3}{6r^3} + \left( \vec{r} \cdot \dot{\vec{r}} \right) \frac{\tau_i^4}{4r^5} \quad (4)$$

Since this equation is non-linear, iterative techniques are frequently used to solve it. Finding the velocity vector makes it possible to compute the orbital parameters of the celestial body, such as its semi-major axis, eccentricity, inclination, and other crucial values.

$$\vec{r}_2 = a_1 \vec{r}_1 + a_3 \vec{r}_3 \quad (5)$$

$$\dot{\vec{r}}_2 = b_1 \vec{r}_1 + b_3 \vec{r}_3 \quad (6)$$

For the purpose of determining the orbital element, the computed vectors are not in the correct coordinate system. The algorithm needs to convert coordinates from the equatorial to the ecliptic plane in order to account for Earth's tilt. In order to take into account the Earth's dynamic tilt, the obliquity must first be found with the year given. Once it has been determined, the orbital element equations can be solved by applying and substituting the coordinate transform. (Gronchi 2004) The orbital elements are described using the following equations:

$$a = \frac{1}{\frac{2}{r} - \frac{v^2}{\mu}} \quad (7)$$

$$e = \sqrt{1 - \left( \frac{h^2}{\mu a} \right)} \quad (8)$$

$$i = \arccos \left( \frac{h_z}{h} \right) \quad (9)$$

$$\sin(\Omega) = \left( \frac{h_x}{h \sin(i)} \right) \quad (10)$$

$$\omega = U - \nu \quad (11)$$

$$M = E - e \sin(E) \quad (12)$$

In these equations,  $r$  is the radial distance,  $v$  is the velocity,  $\mu$  (mu) is the standard gravitational parameter,  $h$  is the specific angular momentum,  $h_z$  is the component of specific angular momentum vector in the direction of the z-axis,  $h_x$  is the component in the direction of the x-axis,  $U$  is the argument of latitude,  $\nu$  (nu) is the true anomaly,  $E$  is the eccentric anomaly, and  $e$  is the eccentricity.

Although Gauss's method gives an initial estimate of the orbit, contemporary methods usually involve additional observations and sophisticated techniques, such as least squares fitting, to further refine the orbit. (Farae et al 2021)

### B. Finding x,y,z

By using a Python script, the 6 orbital parameters were used to calculate the x,y,z coordinates of the asteroid at certain epochs. This allowed us to plot the orbits of the seven different asteroids. A set of 100 different dates with 20 day intervals were generated using a date generating python script.

Durham is represented by an observer object that is created with precise geographic coordinates (longitude and

latitude), elevation, temperature, and observation date. Durham is located at latitude 54:46:01 and longitude -1:34:24. The asteroid's (minor body's) orbital parameters are read from a file. Among these parameters are: Mean anomaly, Argument of periaxis, Longitude of ascending node, Inclination, Eccentricity, Semi-major axis, Absolute magnitude, Slope parameter and the epoch of the mean anomaly. For the Durham observer, the "Elliptical Body" object for the minor body is computed, which includes the right ascension and declination. After that, the position is transformed into latitude and longitude, or ecliptic coordinates. The minor body's distance from Earth is computed. The minor body's Cartesian coordinates ( $x$ ,  $y$ , and  $z$ ) are calculated using the ecliptic coordinates and Earth distance. In a similar manner, the position of the sun is determined for the same date and observer. After converting the sun's position into ecliptic coordinates, it is converted into Cartesian coordinates ( $x$ ,  $y$ , and  $z$ ).

$$x_{\text{minor}} = d_{\text{minor}} \cdot \cos(Lat_{\text{minor}}) \cdot \cos(Long_{\text{minor}}) \quad (13)$$

$$y_{\text{minor}} = d_{\text{minor}} \cdot \cos(Lat_{\text{minor}}) \cdot \sin(Long_{\text{minor}}) \quad (14)$$

$$z_{\text{minor}} = d_{\text{minor}} \cdot \sin(Lat_{\text{minor}}) \quad (15)$$

$$x_{\text{sun}} = d_{\text{sun}} \cdot \cos(Lat_{\text{sun}}) \cdot \cos(Long_{\text{sun}}) \quad (16)$$

$$y_{\text{sun}} = d_{\text{sun}} \cdot \cos(Lat_{\text{sun}}) \cdot \sin(Long_{\text{sun}}) \quad (17)$$

$$z_{\text{sun}} = d_{\text{sun}} \cdot \sin(Lat_{\text{sun}}) \quad (18)$$

In these equations,  $d_{\text{minor}}$  and  $d_{\text{sun}}$  are the distances to the minor body and the Sun, respectively,  $Lat_{\text{minor}}$  and  $Lat_{\text{sun}}$  are the ecliptic latitudes, and  $Long_{\text{minor}}$  and  $Lat_{\text{sun}}$  are the ecliptic longitudes of the minor body and the Sun.

The date, ecliptic coordinates, and Cartesian coordinates of the Sun and minor body are stored in a list by the script. These coordinates for every date are printed once all the dates have been processed. The script computes and transforms coordinates into a format suitable for additional astronomical analysis or visualization by utilizing the observer's location and the orbital elements of the celestial body. For objects in the solar system, the ecliptic coordinate system is especially helpful. Converting these coordinates to Cartesian coordinates ( $x$ ,  $y$ ,  $z$ ) offers a more intuitive understanding of the body's position in three-dimensional space with respect to Earth.

### C. Parallax

Using the asteroid Marion, the astronomical unit (AU) was determined by simultaneously observing from two different places on Earth, namely Durham and La Palma. The apparent shift in motion, or parallax angle, was found by

taking simultaneous photos of Marion from both locations at the same time. The various lines of sight from each observation point on the surface of the Earth give rise to this angle.

The distance between Durham and La Palma serves as the baseline for this parallax measurement rather than the Earth's diameter. The geographic coordinates (latitude and longitude) of the two locations can be used to calculate this baseline. The parallax angle seen between the two simultaneous images, once the baseline is known, enables the calculation of the distance to Marion  $d_{\text{Earth-Marion}}$  using trigonometric relations. Specifically, the distance to Marion can be calculated using the formula:

$$d_{\text{Earth-Marion}} = \frac{d_{\text{baseline}}}{2 \sin(\frac{\theta}{2})} \quad (19)$$

where  $d_{\text{baseline}}$  is the baseline and  $\theta$  is the parallax angle. It is easy to determine the value of 1 AU in absolute terms if you know the distance in kilometers between Earth and Marion and the distance in AU from Marion to the Sun. The average distance between Marion and the sun is the semi-major axis  $a$ . (Vanderbei, Belikov 2007) We can therefore estimate our own value of the AU by employing basic geometric and trigonometric techniques that are akin to those employed by Atkinson in 1930.

$$1 \text{ AU} = \frac{d_{\text{Sun-Marion}}}{d_{\text{Earth-Marion}}} \quad (20)$$

where  $d_{\text{Sun-Marion}}$  is the mean average distance from Marion to the sun.

(Atkinson 1982)

#### D. Error Analysis

The discrepancies between celestial objects' observed and model-predicted positions—such as asteroids—are known as residuals in astrometry. These residuals are computed by the European Space Agency's Gaia astrometry software, which is a component of the data processing pipeline for the Gaia mission. The software used by Gaia to detect asteroids locates them in the image by comparing their position to these catalogued stars. The program then makes a comparison between the observed and predicted positions of the asteroid, which are determined using the asteroid's known orbit and the most recent model of object motion in space (Eggl et al 2020). Astrometric data on about 1.7 billion sources have been gathered by the Gaia mission since 2013 (Gaia Collaboration et al., 2018). The positions of our asteroids along with their residuals were calculated using this method. The jackknife method is a popular re-sampling technique that computes an estimate from sub-samples of the available sample and yields estimates of the bias and a standard error. In the jackknife test, if the data set contains a total of  $N$  members, we perform leave-one-out cross-validation, where the predictor is trained on  $(N - 1)$  training examples and tested on the remaining 1 data point. Following that, the procedure is repeated  $N$  times, at which point each sample's predicted label is determined. (Sinhary 2010). To calculate the errors on the orbital parameters outputted by Findorb the jackknife

method was used. Where  $N$  is the number of ground-based observations. Once calculated the outliers out of each set were extracted. As for the error in parallax reduction due to uncertainties in the position of the observer. In the case of a small angle  $\theta$ , one can use

$$\Delta^2 = \frac{\Delta RA^2 + \Delta Dec^2}{p} \quad (21)$$

(Thuillot et al 2015).

Propagating the error on equation 20 for a function of the form  $Z = A/B$ :

$$\frac{\Delta AU}{AU} = \sqrt{\left( \frac{\Delta d_{\text{Earth-Marion}}}{d_{\text{Earth-Marion}}} \right)^2 + \left( \frac{\Delta d_{\text{Sun-Marion}}}{d_{\text{Sun-Marion}}} \right)^2} \quad (21)$$

(Hughes and Hase 2010).

### III. RESULTS

Over the course of three months, our team successfully conducted observations of seven distinct asteroids, utilizing the advanced telescopes at Durham University's Physics Department. The following summarizes the key findings and data gathered from this project. The results focus on the three asteroids: Helio, Aneas and Kallisto. This is due to the differences in their location, spectral type and orbital period as can be seen in Table 1. By analyzing these three asteroids we were able to compare between an outer belt asteroid, middle belt asteroid, and a Jupiter trojan. From the images, we meticulously extracted the longitudinal and latitudinal coordinates of each asteroid. This data, presented in Table 2, forms the basis of our subsequent orbital analysis. Not much information can be extracted just by viewing values of RA and Dec. That is why further analysis was required. However, by plotting these coordinates, we are able to visualize their path. Figure 4 shows the positions of the asteroids in the sky throughout our observations. Notable observations include how far Helio and Kallisto travelled across the sky over the course of the project and how close they are to each other. However, Aneas was moving much slower and is moving in a different direction than the other main belt asteroids.

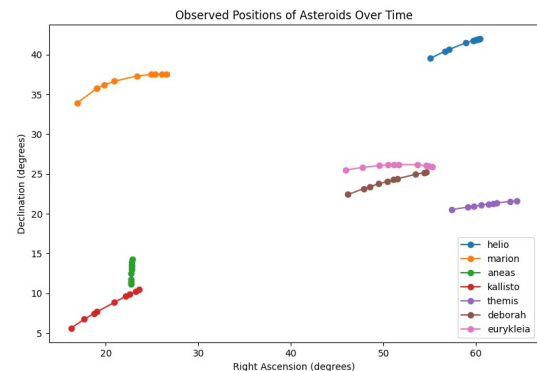


**FIG. 4:** Asteroid positions in the sky

When FindOrb calculated the orbital parameters of each asteroid, the jackknife method was employed to find the standard errors on these values, as can be seen in table 2.

Asteroid	$a \pm \text{error}$	$e \pm \text{error}$	$i \pm \text{error}$	$\Omega \pm \text{error}$	$\omega \pm \text{error}$	$M \pm \text{error}$
Helio	$3.21 \pm 2.94 \times 10^{-5}$	$0.144 \pm 4.58 \times 10^{-5}$	$26.07 \pm 1.72 \times 10^{-3}$	$264.1 \pm 1.99 \times 10^{-3}$	$177.3 \pm 0.06$	$340 \pm 0.124$
Marion	$3.05 \pm 4.18 \times 10^{-4}$	$0.149 \pm 6.31 \times 10^{-4}$	$17 \pm 0.002$	$313 \pm 0.02$	$146 \pm 0.237$	$313 \pm 0.07$
Kallisto	$2.67 \pm 5.51 \times 10^{-5}$	$0.172 \pm 1.31 \times 10^{-4}$	$8.27 \pm 1.31 \times 10^{-4}$	$205.08 \pm 1.31 \times 10^{-4}$	$55.7 \pm 0.389$	$114 \pm 0.389$
Deborah	$2.82 \pm 0.923$	$0.05 \pm 4.95 \times 10^{-5}$	$6.01 \pm 4.95 \times 10^{-5}$	$267 \pm 4.95 \times 10^{-5}$	$357 \pm 0.923$	$138 \pm 1.03$
Themis	$3.15 \pm 0.002$	$0.126 \pm 0.008$	$0.74 \pm 0.005$	$36.4 \pm 0.131$	$105 \pm 1.27$	$287 \pm 0.818$
Eurykleia	$2.88 \pm 0.002$	$0.05 \pm 0.02$	$6.97 \pm 0.01$	$7.01 \pm 0.08$	$123 \pm 7.16$	$287 \pm 6.47$
Aneas	$5.23 \pm 0.001$	$0.111 \pm 0.006$	$0.002 \pm 16.7$	$247 \pm 0.03$	$48.5 \pm 2.13$	$176 \pm 1.34$

TABLE II: Orbital Parameters of Observed Asteroids

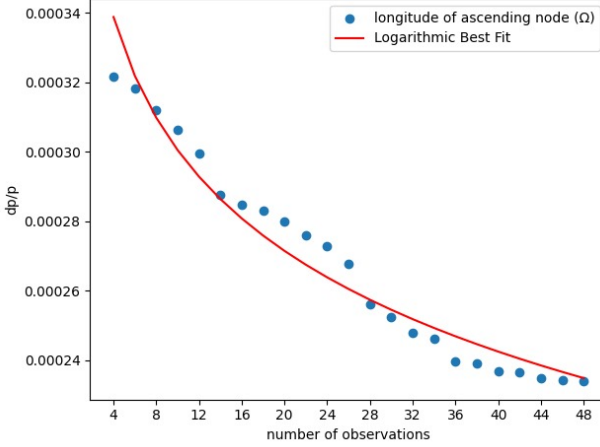


FIG. 5: Fractional uncertainty on longitude of ascending node for 48 observations with logarithmic line of best fit

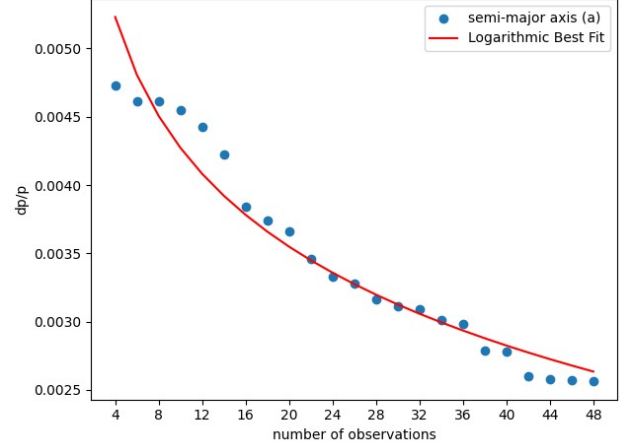


FIG. 6: Fractional uncertainty on semi-major axis for 48 observations with logarithmic line of best fit.

Since Findorb was used to determine the orbital parameters, it is imperative to demonstrate its dependability. How were the consistency and accuracy evaluated? by graphing the number of observations against the fractional uncertainty. This served to illustrate how the orbital parameters predicted by the software improved with additional observational data. These values, which were fed into Findorb at intervals of 4, were started with 4 observations and continued up to 48 observations. The observations were processed by the software, which also produced orbit predictions. For comparison, a baseline orbit estimate was created. The fractional uncertainty in the orbit parameters was computed for every prediction. This involved dividing the computed value by the absolute uncertainty. The plot offered a graphic depiction of the software's functionality at various data points.

This kind of analysis was performed to determine how the accuracy of orbital parameters calculated by the software FindOrb is impacted by the gathering of additional data. Figures 5 and 6 show the calculated longitude of ascending node and semi-major axis of the asteroid Aneas. The fractional uncertainty of the estimated parameters falls as the number of observations rises. This shows that increasing the number of observations that FindOrb receives can result in orbital parameter estimates that are more accurate. A logarithmic decrease in fractional uncertainty with the number of observations is indicated by the best-fit line. This is typical of observational astronomy, where results tend to be less noisy when more data are added. Because the data is logarithmic, it is possible that each additional observation greatly increases the precision at first, when there are few observations. The contribution of each new observation

to increasing precision decreases as the number of observations increases. Plots also imply that the precision achievable, independent of the number of observations, may have an asymptotic limit. This limit might result from systematic uncertainties that are too great to be overcome by merely increasing the number of observations. An ideal amount of data for using FindOrb to calculate these parameters may exist at a point where adding more observations does not significantly increase the precision. This aids in resource allocation by preventing the use of computational power and time on tasks with diminishing returns. Additionally important is the caliber of each observation. Raising the number of observational data points may not yield appreciable improvements in orbital parameter estimation if those points are subject to systematic errors. (Pourbaix 2002)

The culmination of our project involved the development of a Python-based predictive model. This model efficiently processes the orbital parameters to generate the x, y, z coordinates of the asteroids at any given date and time. The accuracy of this model was validated against known asteroid positions, with a high degree of correlation observed.

The plotted trajectories of the asteroids, as generated by the model, provide a clear visualization of their orbits. These plots reveal the dynamic and complex nature of asteroid's motion within our solar system. Figure 7 shows the orbits of these seven asteroids plotted by allowing the Python program to output x,y,z coordinates for 100 different dates starting at 20 day intervals.

The sun is at the centre of the orbits but not the plot because the coordinates of the asteroids are calculated relative to the sun. By using equations 16, 17, and 18, the respective sun coordinates were also calculated. Aneas's orbit is

larger than the others because it is technically classified as a Jupiter Trojan.

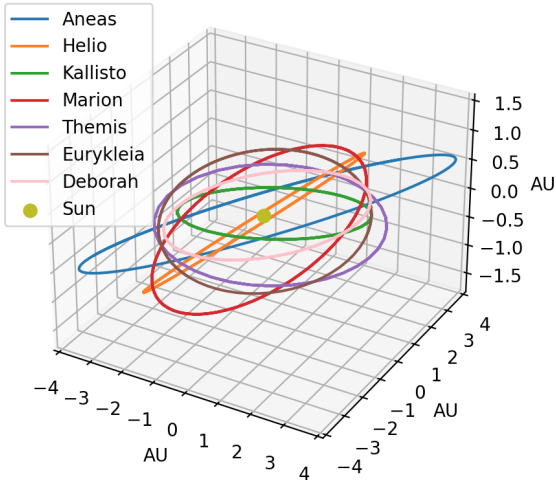


**FIG. 7:** The Orbits of 7 Asteroids

The final part of this project was to calculate the distance to Marion and consequently utilize it to determine a value of 1 AU.

Parameter	Value
$d_{\text{Earth-Marion}}$	$2.2 \pm 0.5 \text{ AU}$
Baseline, $b$	3169.51km
Parallax angle, $\theta$	$9.74 \times 10^{-11} \pm 0.81 \text{ arcseconds}$
$d_{\text{Sun-Marion}}$	$3.05 \pm 4.18 \times 10^{-4} \text{ AU}$
Calculated AU value	$1.375 \pm 0.227 \text{ AU}$

**TABLE III:** Astronomical measurements for calculating AU

According to the National Institute of Standards and Technology, the literature value of 1 Astronomical Unit is 149 597 870 700km (the average distance between the Earth and Sun).The percentage deviation is

$$\frac{56,114,161.3}{149,597,870,700} \times 100 = 37.5\% \quad (22)$$

Which means our value is 37.5 % greater than the standard value.

The project achieved its objectives of capturing and analyzing asteroidal data, leading to a deeper understanding of their orbital dynamics. The implications of this study extend to future space missions and contribute to our knowledge of solar system formation, as discussed in the following section.

#### IV. DISCUSSION

At 5.23 AU, Aneas has the highest semi-major axis. Generally speaking, an asteroid with a higher semi-major axis orbits farther from the Sun. Since Trojans are found close to Jupiter's orbit, which is located about 5.2 AU from the Sun, this is consistent with Aneas being a Jupiter Trojan. At 0.149, Marion has the highest eccentricity. Eccentricity quantifies how far an orbit deviates from a perfect circle. An orbit that is longer is indicated by a higher value. Compared to the other listed asteroids, Marion's orbit appears

to be less circular due to its relatively higher eccentricity. At 26.07 degrees, Aneas has the highest inclination as well. The inclination of an asteroid is its tilt with respect to the ecliptic, the plane of the solar system. Due to Aneas's high inclination, its orbit is tilted more than the orbits of the other asteroids. This tilt may be the result of previous collisions or gravitational interactions. Marion has the highest ascending node longitude, measuring 313 degrees. The point in the orbit where the asteroid crosses the ecliptic plane from south to north is known as the ascending node's longitude. An asteroid's orbit is further along at a point indicated by a higher value. At 177.3 degrees, Helio has the highest perihelion argument. The angle between an asteroid's ascending node and its closest approach to the Sun is known as the perihelion argument. Given its high value, Helio appears to be further along in its perihelion.

Errors, both random and systematic, can affect asteroid observations and the orbital parameters and positions that are subsequently calculated.

Systematic errors, such as instrumental bias: Consistent offsets from the true values can be introduced by flaws in the telescope's optics, detector sensitivity, or calibration. Photon Noise: Measurement variability may arise from intrinsic fluctuations in the quantity of photons detected, also known as quantum noise. Random fluctuations in the asteroid's observed position can be caused by flaws in the telescope's tracking system. Dust particles collecting on the surface of the telescope can also cause irregularities in the images. That is why it is essential to use flats or mosaic images that cancel out these anomalies. Minor discrepancies in the timing of observations may cause measured position errors. Examples include taking images of Marion at the same time to calculate the parallax angle. Random errors in the observed position of the asteroid can result from inaccurate reference star positions used for calibration. Generally speaking, the more accurate the observation, the more accurate the star catalog. Asteroid astrometry is highly biased, despite the widespread belief that observation errors have a zero mean. This bias may be caused by systematic errors in the star catalogs that are used to minimize astrometry (Farnocchia, 2015). Residuals can be calculated for the observed position and the expected position of the asteroid. This is based on the number and brightness of stars that are visible in the reference frame. The more stars are visible, the more accurate the asteroid position. These differences can be seen in figure 8.

That is why positional data of our asteroids and data extracted from JPL were compared. Figures 9 and 10 residual plots that contrast the asteroid Aneas's and Helio's actual position with those predicted by JPL's HORIZONS system. It was used to assess how accurate the observations are. Plotting the disparities (residuals) between observed positions and JPL predictions for Right Ascension (RA) and Declination (Dec) is done. The residuals are expressed in arcseconds. This represents the residuals' median in both Dec and RA. As seen on the plot, it indicates the typical systematic error that exists in the data, with a median offset of [-0.18, -0.185 arcsec]. The typical size of the residuals is indicated by the root mean square (rms) of the differences in RA and Dec, which is given as [0.18, 0.16 arcsec]. This is a measure of the scatter in observations. Assuming a bivariate normal distribution, the concentric dashed ellipses show the 1-sigma (68.27%), 2-sigma (95.45%), and 3-sigma (99.73%) confidence intervals for the residual dis-

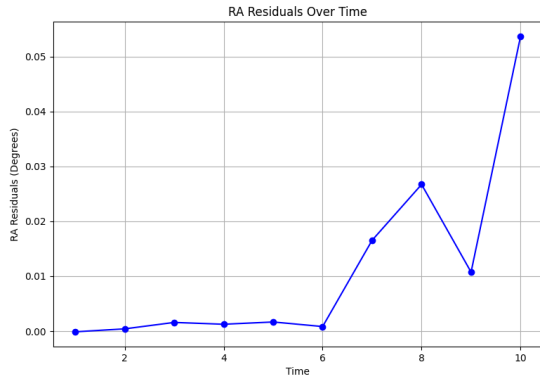


**FIG. 8:** Residuals caused by using star catalogue to extract Helio's position.

tribution. The innermost ellipse indicates the likelihood that new observations will fall within these probability regions, which are represented by these ellipses.

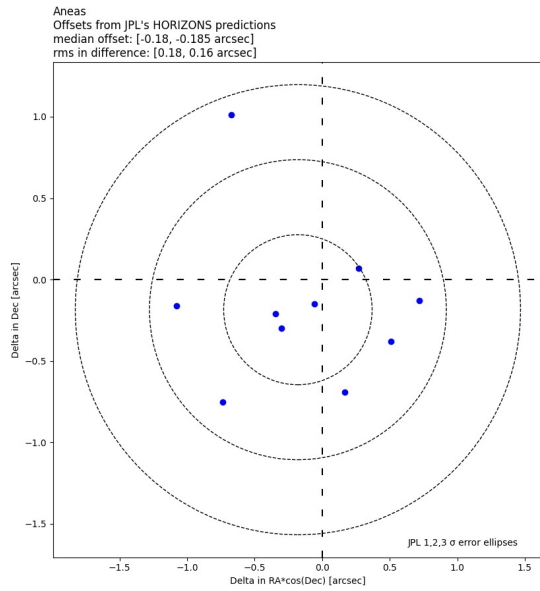


**FIG. 9:** Aneas positions predicted by the JPL Horizons On-line Ephemeris are compared with the measured astrometric positions. Error ellipses represent the formal  $\pm 1, 2$ , and  $3$  standard-deviation uncertainties for JPL

The software used throughout the project also poses a source of uncertainty. Any prejudices or restrictions in software, such as FindOrb's algorithms, that were used to compute the orbital parameters. That is plots 5 and 6 of the fractional uncertainty were crucial, to better understanding and assessing this risk. The values of the calculated orbital parameters were compared to those generated by JPL. Their percentage difference can be seen as follows for three of the orbital parameters across all asteroids:

According to these bar graphs, the computed values come very close to the JPL values. This therefore indicates that 9-10 observations for each asteroid was a good choice since it allows us to calculate their orbital elements to such a high degree of accuracy.

Due to the sensitive dependence on initial conditions,

small errors in the initial position and velocity vectors can result in larger errors in the plotted orbit. Relativistic forces should also be taken into consideration. Errors in the orbital solution can be caused by poorly or non-existent modeled forces, such as the Yarkovsky effect or non-gravitational forces. When small bodies in the solar system, like asteroids, are subjected to the Yarkovsky effect, it can have a discernible long-term impact on their orbits. When an object absorbs solar radiation and re-emits it as heat, a non-gravitational force is created. This re-emission has the potential to change the object's trajectory by exerting a slight but constant push due to the conservation of momentum. The Yarkovsky effect is particularly significant in the context of this research, which involves modeling orbits and asteroid observations, for the following reasons: Yarkovsky effect can cause asteroids to deviate significantly from the expected path, which is important for long-term impact risk assessments, from their predicted orbits that are calculated using gravity alone (Denise Hung et al 2023). "An asteroid in resonance experiences enhanced gravitational perturbations from Jupiter, which can cause regular variations in its orbital elements. The extent of these variations depends on the asteroid's location within the resonance, which is, in turn, determined by the starting conditions." (Catling, Leovy 2007)

There are a couple things to take into consideration when wanting to improve on this project. Instrument calibration on a regular basis can help lower systematic errors. Some systematic biases can be reduced by processing raw observational data using advanced data reduction techniques. Random error can be minimized by averaging data from several observations. Systematic errors in orbital calculations can be minimized by refining the physical model of the asteroid's motion, taking into account perturbations from other bodies and non-gravitational forces. Additional observations were made using a different star catalogue with

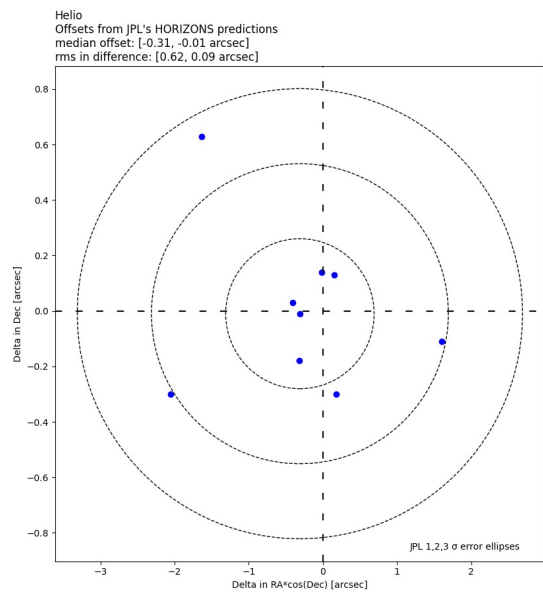


**FIG. 10:** Helio positions predicted by the JPL Horizons On-line Ephemeris are compared with the measured astrometric positions. Error ellipses represent the formal  $\pm 1, 2$ , and  $3$  standard-deviation uncertainties for JPL

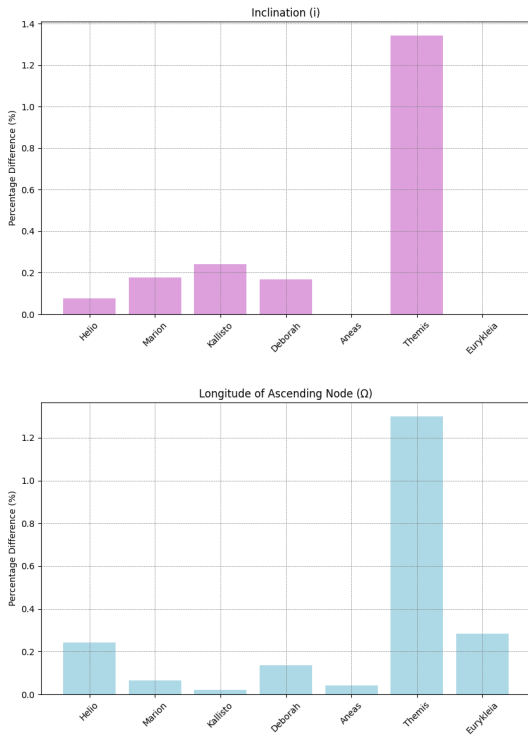


**FIG. 11:** Percentage difference between computed orbital parameters and those generated by JPL

a larger collection of reference stars. Improvements to our parallax calculation are also crucial. The precise positions of Earth and the asteroid in their orbits at the moment of the parallax measurement could also be taken into account to improve this computation. This can be achieved by accounting for the true anomaly of the Earth and the asteroid, which is their actual orbital position with respect to their closest point to the Sun (perihelion). A more precise estimate of the AU can be obtained by modifying the distance to the asteroid for these orbital positions. Once the exact distance between Earth and Marion is known, the distance between Marion and the Sun in astronomical units can be calculated using Kepler's third law. Since the orbital period's square and the cube of its period are correlated by law, this relationship gives the distance from the Sun to Marion in terms of AU.

FindOrb utilizes Gauss' Method of Orbital Determination. This mathematical method is ideal for three observations. However, taking into account the fractional uncertainty plots, we know that the error in values decreases as the number of observations increases. What should be considered when choosing the number of observations for each asteroid? In order to use Gauss's method, observations must be dispersed over time. Three closely spaced observations may not reveal as much about the orbit as three more widely separated observations. In these kinds of situations, ten or more observations may provide a more precise orbit determination. Having more observations adds redundancy, which aids in identifying and minimizing random errors. Statistical techniques can be used to refine the orbital elements and obtain a more dependable result with ten observations. Less observations might be needed for basic orbits that are elliptical or nearly circular. On the other hand, for more intricate orbits, like those that are highly eccentric or affected by non-gravitational forces, having more observa-

tions can be beneficial. More observations mean more complicated calculations when using Gauss's method. Larger numbers of observations are usually manageable with current computing resources, even though three observations may be easier to process computationally. It is simpler to find and eliminate outliers that could distort the orbital elements when there are more observations. When there is a possibility of observational errors, this can be especially helpful.

Determining and tracking the asteroid's orbit with extreme precision is one of the many intricate steps involved in planning a mission to an asteroid. For every type of asteroid, we would approach mission planning differently. We must take into consideration the fact that Anreas is categorized as a Jupiter Trojan when organizing a mission there. Because of Jupiter's strong gravitational pull, Trojans can have complex orbital dynamics and share Jupiter's orbit. As a result, the trajectory of the mission to the Trojan may need to account for the gravitational pull of both Jupiter and the Sun.

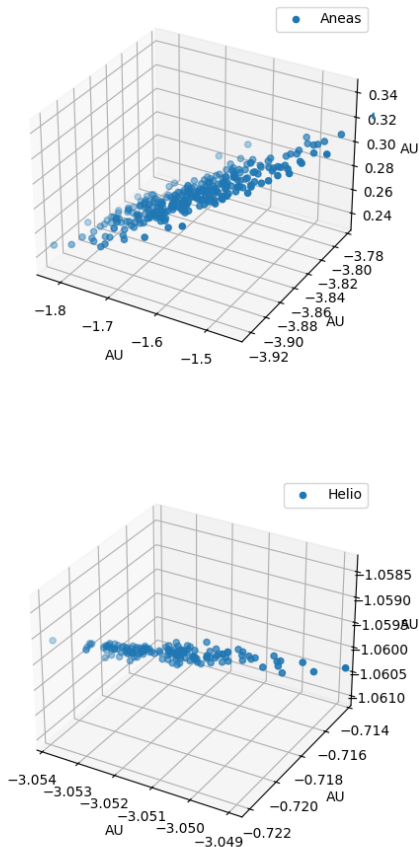


**FIG. 12:** Monte Carlo Method used to vary the orbital parameters by 1-sigma using their uncertainties. 300 possible values generated.

Anreas's position in the Trojan swarm and the Earth's favorable alignment with Jupiter's orbit would determine the launch window. Lastly, the gravitational perturbations from Jupiter and possibly other nearby large Trojans would need to be taken into account when navigating a spacecraft to Anreas. Monte Carlo simulations were used to vary the asteroid's known orbital parameters within a 1-sigma uncer-

tainty, allowing for the simulation of a broad range of potential trajectories. An asteroid's possible future positions were generated as a probability distribution using 300 distinct sets of orbital parameters for the same day. The technique offers a probability estimate of the asteroid's potential location in the future. Thus making it useful in orbital mechanics and space mission trajectory planning. Based on the fluctuations of its orbital parameters, this plot displays a 3D scatter of potential locations for the asteroid Aneas.

The uncertainty in its trajectory caused by the Yarkovsky effect and other perturbations is represented by the spread in the x, y, and z directions. Planning a rendezvous mission requires taking into account the relatively narrow range of positions that are suggested by the dense cluster of points. A more compact distribution of possible positions is depicted in the plot for the outer main belt asteroid Helio, suggesting a higher degree of confidence in its orbital parameters. The smaller spread may result from more accurate measurements or from being less vulnerable to non-gravitational forces, which makes mission planning easier.

## V. CONCLUSION

Thorough examination of the chosen main belt asteroids has provided important new information about the dynamical state of the main minor planet repository in our solar system. Aneas's high semi-major axis and inclination reflect the intricate gravitational interactions with the gas giant and represent the variety of features found in Jupiter Trojans. . Using parallax measurements on the asteroid Marion it was found that the AU value was only 37.5 % higher than the standard value. It was measured as  $1.375 \pm 0.227$  AU or 205 712 032 000km. The Monte Carlo method used in this project has emphasized how crucial it is to include statistical tools in order to account for observational uncertainties. To further solve the mysteries of the future, research endeavors should persist in incorporating probabilistic models and longitudinal observational data. To further solve the mysteries surrounding the formation and evolution of the main belt, future research should continue to integrate probabilistic models with long-term observational data. We are getting closer to discovering the mysteries of the early solar system and its processes of development as we learn more about these celestial objects.

## VI. REFERENCES

1. de la Fuente Marcos, C., de la Fuente Marcos, R. (2022) 'Recent arrivals to the main asteroid belt', *Celestial Mechanics and Dynamical Astronomy*, 134(38). doi: 10.1007/s10569-022-10094-4.
2. Raymond, S.N., Nesvorný, D. (2021) 'Origin and dynamical evolution of the asteroid belt'. Available at: <https://hal.science/hal-03419396> (Accessed: Date).
3. Liu, S., Wu, Z., Yan, J., Gao, J., Huang, H., Cao, J., Li, X., Barriot, J.-P. (2023) 'Orbital eccentricity and inclination distribution of main-belt asteroids—The Statistical model revisited', *Icarus*, 404. doi: 10.1016/j.icarus.2023.115650.
4. Martin, R.G. and Livio, M. (2022) 'Asteroids and Life: How Special Is the Solar System?', *The Astrophysical Journal Letters*, 926(L20). doi: 10.3847/2041-8213/ac511c.
5. Michel, P. (2014) 'Formation and Physical Properties of Asteroids', *Elements*, 10(1), pp. 19–24. doi: 10.2113/gselements.10.1.19.
6. Carruba, V., Nesvorný, D., Aljbaae, S., Domingos, R.C., Espinoza, M.H. (2016) 'On the oldest asteroid families in the main belt', *Monthly Notices of the Royal Astronomical Society*. doi: 10.1093/mnras/stw533.
7. Catling, D.C., Leovy, C. (2007) , *Encyclopedia of the Solar System* (Second Edition). doi: 10.1016/B0122274105000314.
8. Thabet, M. (2013) 'Measuring Distances in Space', *SSRN Electronic Journal*. doi: 10.2139/ssrn.2355164.
9. Vanderbei, R., Belikov, R. (2007) 'Measuring the astronomical unit from your backyard', *Sky and Telescope*, 113(1), pp. 91–94. Available at: <https://vanderbei.princeton.edu/tex/MeasureAU/ms.pdf> (Accessed: Date).
10. Siebert, H. (2005) 'The Early Search for Stellar Parallax: Galileo, Castelli, and Ramponi', *Journal for the History of Astronomy*, 36, pp. 251–271. doi: 10.1177/002182860503600301.
11. Omodaka, T. 'VERA Project: Measuring Our Milky Way Galaxy'. DOI:10.1017/S1743921305001663
12. Atkinson, R.d'E. (1982) 'Abstract', *Journal for the History of Astronomy*. doi: 10.1177/002182868201300201.
13. Eggl, S., Farnocchia, D., Chamberlin, A.B., Chesley, S.R. (2020) 'Star catalog position and proper motion corrections in asteroid astrometry II: The Gaia era', *Icarus*, 339. doi: 10.1016/j.icarus.2019.113596.
14. Gaia Collaboration (2018) 'Gaia Data Release 2. Summary of the contents and survey properties', *Astronomy and Astrophysics*, 616. doi: 10.1051/0004-6361/201833051.
15. Sinharay, S. (2010) 'Jackknife test', in *International Encyclopedia of Education* (Third Edition). doi: 10.1016/B978-0-08-044894-7.00444-8.
16. Thuillot, W. et al. (2015) 'The astrometric Gaia-FUN-SSO observation campaign of 99 942 Apophis', *Astronomy & Astrophysics*, 583. doi: 10.1051/0004-6361/201425603.
17. Raab, H. (2002) 'Detecting and measuring faint point sources with a CCD'. Available at: <http://www.astrometrica.at/Papers/PointSources.pdf>
18. Farae, M., Woo, C., Hu, A. (2021) 'An Improved Approach to Orbital Determination and Prediction of Near-Earth Asteroids: Computer Simulation, Modeling and Test Measurements'. Available at: <https://www.semanticscholar.org/paper/An-Improved-Approach-to-Orbital-Determination-and-Farae-Woo/64b779e6853478b27ae618b1803fcff482eb9739>
19. Pourbaix, D. (2002) 'Precision and accuracy of the orbital parameters derived from 2D & 1D space observations of visual or astrometric binaries', *Astronomy & Astrophysics*, 385(2), pp. 686–692. doi: 10.1051/0004-6361:20020149.
20. Hung, D. et al. (2023) 'Detectability of the Yarkovsky Effect in the Main Belt', *Planetary Science Journal*, 4(215). doi: 10.3847/PSJ/ad0226.
- Hughes, I. and Hase, T. (2010). *Measurements and their Uncertainties: A Practical Guide to Modern Error Analysis*. 1st ed

## VII. APPENDIX

Asteroids	Mean Anomaly	JPL Value	Percentage Difference
Helio	339.33	85.88	119.2116836
Marion	313.23	110.16	95.92574222
Kallisto	113.96	135.12	16.99052513
Deborah	137.78	246.66	56.6434294
Aneas	175.9	188.45	6.888980376
Themis	286.62	157.92	57.90255095
Eurykleia	286.71	347.51	19.17315758

**TABLE IV:** Percentage Difference of Mean Anomaly for Asteroids

Asteroids	Argument of Periapsis	JPL Value	Percentage Difference
Helio	177.25	178.054	0.4525701934
Marion	145.8655	146.18	0.2153773984
Kallisto	55.74	55.48	0.467541809
Deborah	357.21	356.98	0.06440863076
Aneas	48.48	51.17	5.398896136
Themis	105	106.86	1.755876522
Eurykleia	123.46	121.06	1.963029609

**TABLE V:** Percentage Difference of Argument of Periapsis for Asteroids

Asteroids	Longitude of Ascending Node	JPL Value	Percentage Difference
Helio	264.07	264.71	0.242066644
Marion	312.75	312.95	0.06392840019
Kallisto	205.08	205.12	0.01950268162
Deborah	267.41	267.77	0.1345341754
Aneas	247.23	247.33	0.04043998706
Themis	36.39	35.92	1.299958512
Eurykleia	7.01	7.03	0.2849002849

**TABLE VI:** Percentage Difference of Longitude of Ascending Node for Asteroids

Asteroids	Inclination	JPL Value	Percentage Difference
Helio	26.07	26.09	0.07668711656
Marion	16.98	17.01	0.1765225066
Kallisto	8.27	8.29	0.2415458937
Deborah	6.01	6	0.1665278934
Aneas	16.66	16.66	0
Themis	0.74	0.75	1.342281879
Eurykleia	6.97	6.97	0

**TABLE VII:** Percentage Difference of Inclination for Asteroids

Asteroids	Eccentricity	JPL Value	Percentage Difference
Helio	0.144	0.146	1.379310345
Marion	0.149	0.148	0.6734006734
Kallisto	0.172	0.175	1.729106628
Deborah	0.05	0.05	0
Aneas	0.111	0.103	7.476635514
Themis	0.126	0.13	3.125
Eurykleia	0.05	0.04	22.22222222

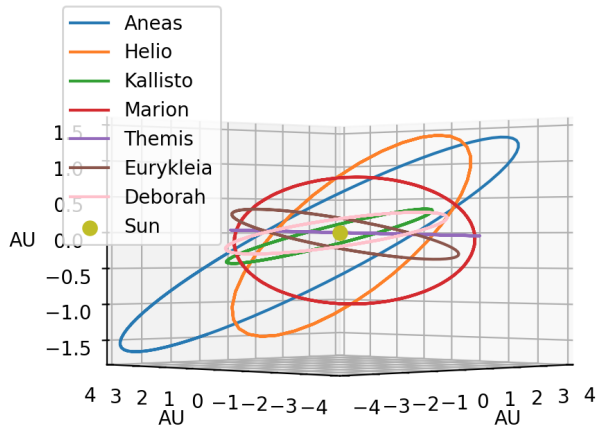
**TABLE VIII:** Percentage Difference of Eccentricity for Asteroids

Asteroids	Semi-major Axis	JPL Value	Percentage Difference
Helio	3.21	3.2	0.3120124805
Marion	3.05	3.04	0.328407225
Kallisto	2.67	2.67	0
Deborah	2.82	2.82	0
Aneas	5.23	5.22	0.1913875598
Themis	3.15	3.14	0.3179650238
Eurykleia	2.88	2.87	0.347826087

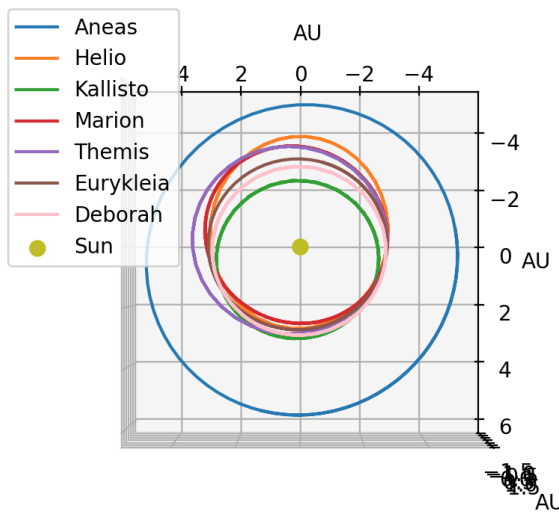
**TABLE IX:** Percentage Difference of Semi-major Axis for Asteroids

Observation Number	Helio			Kallisto			Aneas		
	RA	Dec	Residual	RA	Dec	Residual	RA	Dec	Residual
1	60.4125	41.97	0.153	64.375	21.6378	0.151	342.833333	14.2483	0.297
2	60.25	41.9575	0.184	63.6458	21.5522	0.225	342.125875	13.590475	0.172
3	60.1292	41.9242	0.242	62.2292	21.3533	0.682	341.979167	13.4275	0.151
4	59.8875	41.8497	0.650	61.8833	21.3006	0.524	341.770833	13.1797	0.237
5	59.6917	41.7828	0.539	61.3583	21.2181	0.478	341.65	13.0167	0.627
6	58.9208	41.4911	0.586	60.5833	21.0922	0.165	341.358333	12.5322	0.533
7	57.1	40.6656	0.169	59.7417	20.9506	0.296	341.120833	11.7664	0.582
8	56.6667	40.4428	0.132	59.1042	20.8383	0.601	341.129167	11.4214	0.257
9	55.0833	39.5467	0.456	57.4042	20.5242	0.317	341.195833	11.1639	0.231
10	53.3458	38.395	0.057	-	-	-	342.466667	13.9269	0.619

**TABLE X:** Observational Data for Asteroids Helio, Kallisto, and Aneas

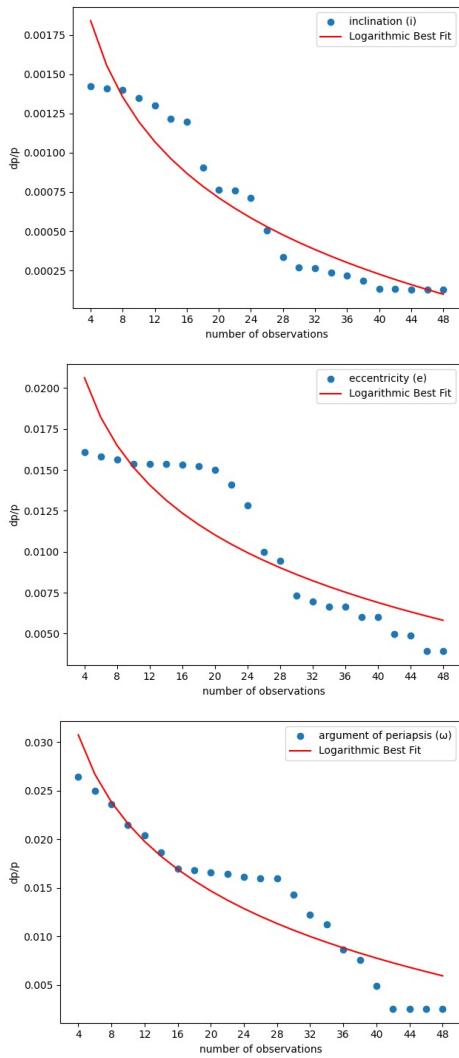


**FIG. 13:** Different perspective of the orbital model plot.  
Elevation= 0 Azimuth= 225



**FIG. 14:** Different perspective of the orbital model plot.  
Elevation=Azimuth=90

Date Observed	Time (UTC) Observed	Telescope	FWHM	Location
01/10/2023	20:08:12-20:16:09	draco-2	2.9-3.8	Durham,UK
05/10/2023	19:21:27-19:42:15	draco-2	3.1-4.7	Durham,UK
9/10/2023	19:46:27-21:06:40	east-16	3.4-4.4	Durham,UK
11/10/2023	20:11:54-21:18:51	east-16	3.4-5.8	Durham,UK
14/10/2023	20:26:35-21:14:59	far east-20	3.0-3.9	Durham,UK
16/10/2023	20:13:19-20:38:04	far east-20	2.8-3.7	Durham,UK
22/10/2023	19:54:59-20:31:31	far east-20	3.4-4.0	Durham,UK
1/11/2023	21:48:12-22:20:55	east-16	5.1-6.6	Durham,UK
03/11/2023	22:37:13-23:23:10	east-16	2.3-4.5	Durham,UK
06/11/2023	20:35:41-21:26:59	east-16	3.1-4.4	Durham,UK
10/11/2023	21:00:32-21:31:02	far east-20	3.4-4.0	Durham,UK
14/11/2023	23:56:35-00:01:35	pt5m	2.2-3.0	La palma,Spain
17/11/2023	21:24:22-01:14:17	pt5m	1.6-3.4	La palma,Spain
24/11/2023	20:35:03-20:50:07	west-14	5.7-6.3	Durham,UK

**TABLE XI:** Observation Logs**FIG. 15:** Fractional Uncertainty plots for the rest of the orbital parameters

## 0.1 Scientific Summary for a General Audience

Ground-based observations were carried out to acquire pictures of seven asteroids during a three-month period. The asteroids' celestial coordinates were extracted from these images for use in a subsequent analysis.

The second stage was to use the 'Findorb' program to infer these objects' orbital characteristics. The six numbers that characterize an asteroid's orbital motion around the sun are called orbital parameters. The reliability of Find-Orb was tested by generating 48 data points from NASA'S JPL and feeding them into the software to visualize how the precision of the calculations varies we increase number of observations. It was proven that increasing number of observations does indeed result in a lower fractional uncertainty until an asymptote is reached and adding observations does not affect the calculations. The analysis section focused on the asteroids: Helio,Aneas and Kallisto. This is due to the difference in location and composition of these asteroids. By analyzing and comparing between the three of them, a broader sense of understanding is achieved. Our efforts resulted in the creation of an advanced predictive model based on Python that can generate exact coordinates for x, y, and z for these asteroids at any given time and date. This model was essential for future space missions, such as asteroid mining projects, in addition to making it easier to visualize their orbits. The project's second goal was to calculate the value of the astronomical unit using the distance to one of our asteroids through a series of calculations. The distance between Earth and the Sun is equal to one astronomical unit (AU). With  $\theta$  calculated using equation (1), it is  $9.7355035 \times 10^{-11} \pm 0.810345$  arcseconds, with the uncertainty on the parallax angle calculated using equation (21). The distance between Durham and La Palma is 3169.51 km or  $1.02716824 \times 10^{-10}$  parsecs. The distance to Marion is  $2.2 \pm 0.5$  AU. A value of  $1.375 \pm 0.227$  AU is obtained from that. Therefore, the value determined for 1 AU is 205 712 032 000 km. According to the National Institute of Standards and Technology, the literature value of 1 Astronomical Unit is 149 597 870 700km (the average distance between the Earth and Sun). Which means our value is 37.5 % greater than the standard value.

The Monte Carlo Method was used to vary the orbital elements that describe the asteroid's motion through space so that 300 different possible positions could be plotted. This allows us to predict where the asteroid might be for future space missions. The project can be further developed by using neural networks for orbit determination of these asteroids. The importance of this project goes beyond simple space travel; it helps solve the puzzles surrounding the early formation of our solar system, which advances our knowledge of cosmic evolution. Future astronomical studies and space missions will be greatly influenced by the information and understanding gathered.